Supporting information

Two-step hybrid photo-thermochemical looping process, using metallic clusters on metal oxide carriers, for very efficient green hydrogen production

Anh Dung Nguyen[a+], David Buceta[b+], Qingqing Wu[c+], Moteb Alotaibi [d], Julian T. Müller[e], Iria R. Arias[b], Albert Gili[f], Maged F. Bekheet[e], Martin Dieste[g], Nerea Davila-Ferreira[g], Fatimah Alhawiti[h], Colin Lambert[c]*, M. Arturo López-Quintela[b]*, Reinhard Schomäcker[a]*

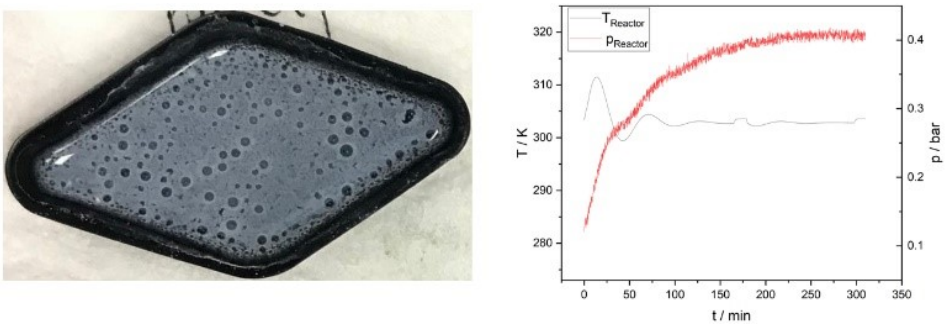

Fig. S1 (a) Evolution of hydrogen, after deposition of Cu AQCs onto TiO_2, (b) Hydrogen evolution in standardized photoreactor without light.

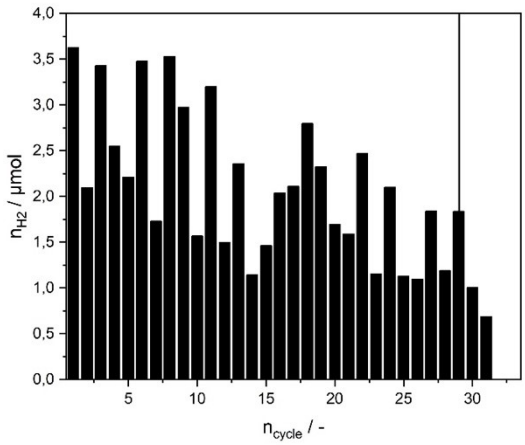

Fig. S2 Volume of H_2 evolved in every cycle with CeO_2/Ag_5 AQCs (0.5 wt% Ag_5), m CeO_2 = 100 mg, $A_{irradiation}$ = 19.6 cm², dV/dt = 10 mL min^{-1}, φ = 30%, T = 773 K, Irradiation source: 200 W Hg (Xe) lamp, λ< 1450nm, $t_{irradiation}$ = 1h, $t_{oxidation}$ = 0.5h.

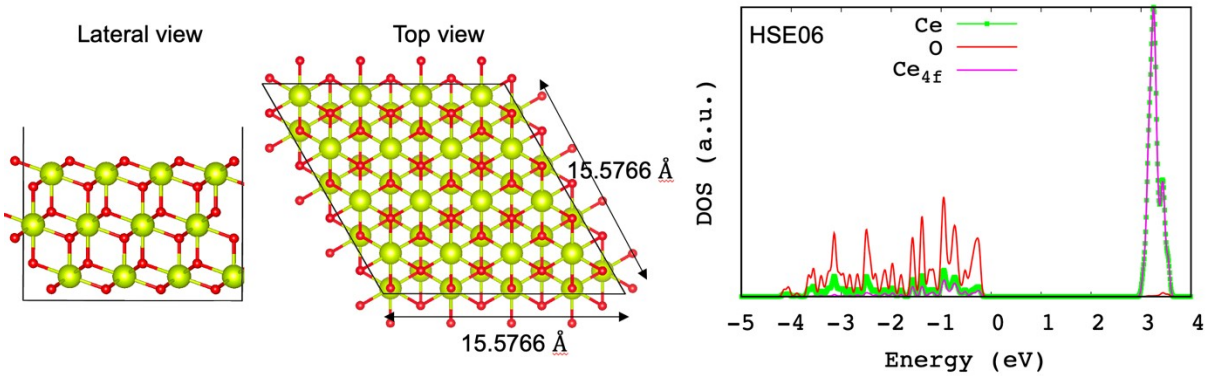

Fig. S3 Model of the pristine $CeO_2(111)$ surface (Lateral and top views) and the corresponding density of states.

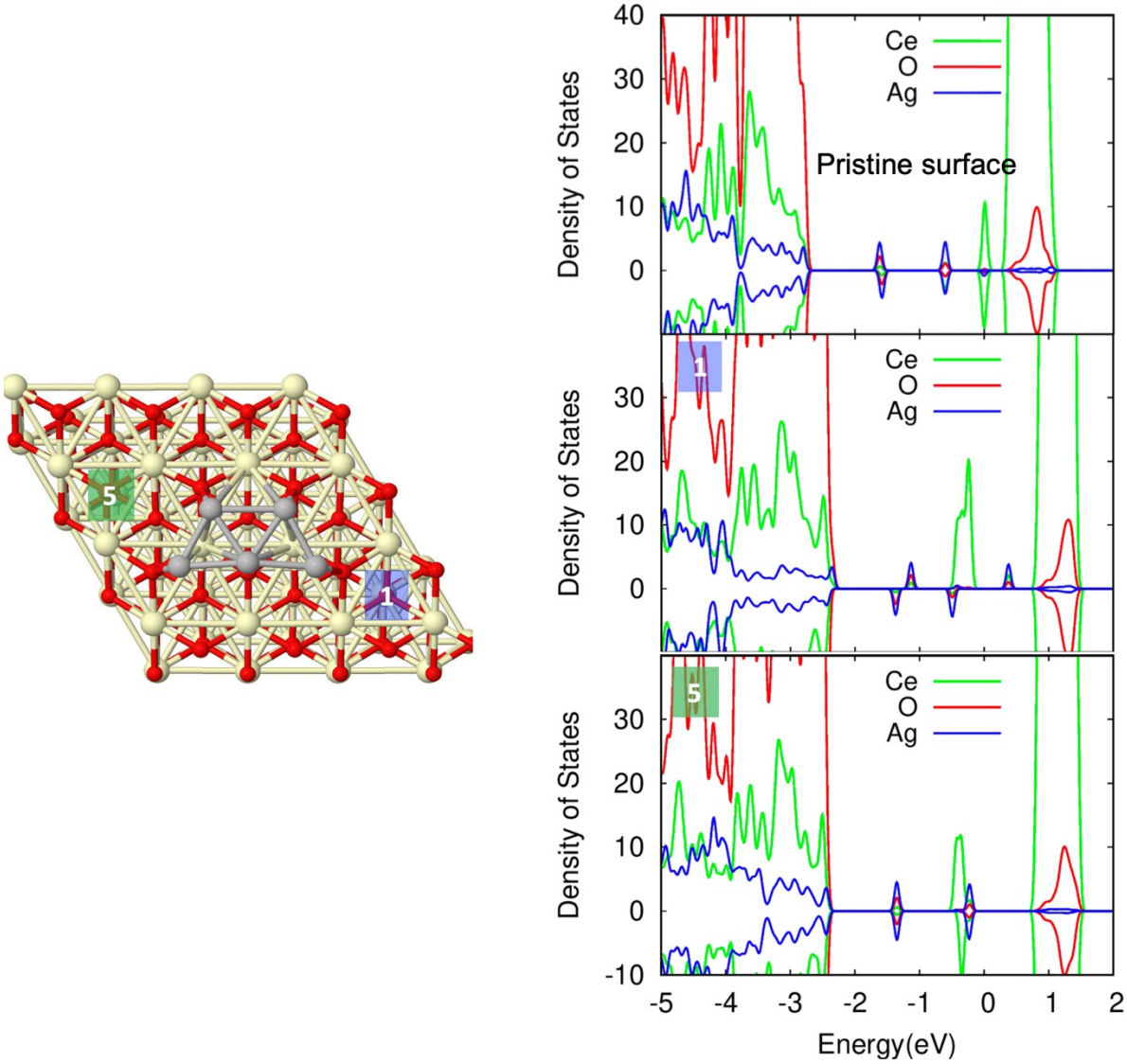

Fig. S4 Geometries and oxygen vacancy positions of a CeO_2 surface with the trapezoidal Ag_5 AQC adsorbed on (left panel) and the corresponding density of states (right panel).

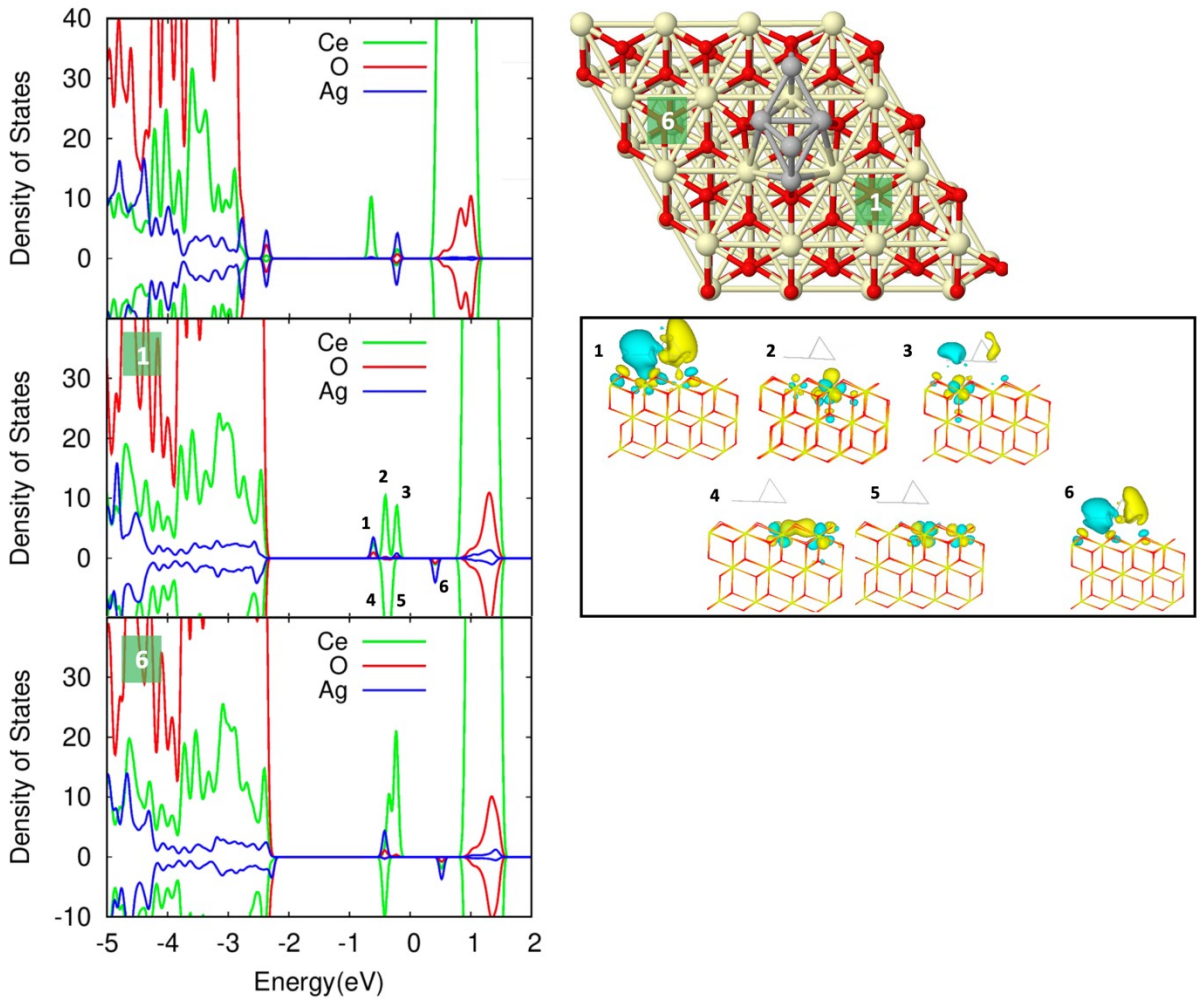

Fig. S5 Geometries and oxygen vacancy positions of a CeO_2 surface with the bipyramidal Ag_5 AQC adsorbed on (right top panel), the corresponding density of states (left panel) and wavefunctions for the structure of position 1 (right bottom panel).

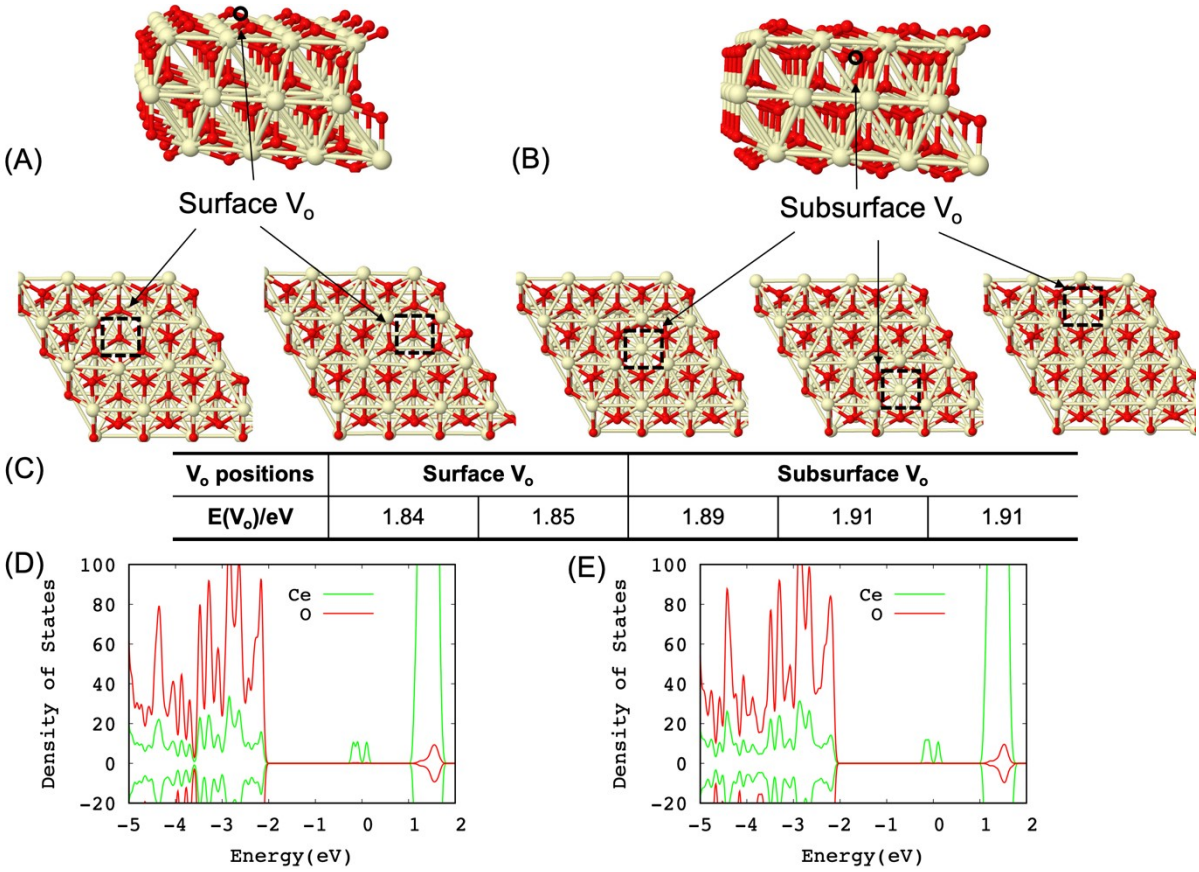

V_o positions	Surface V_o		Subsurface V_o		
$E(V_o)$/eV	1.84	1.85	1.89	1.91	1.91

Fig. S6 Oxygen vacancy formation energy (E_{Vo}) calculations for pure CeO_2 surface. (A) Geometries of surface Vo. (B) Geometries of subsurface Vo. (C) Values of E_{Vo}. (D, E) Density of states corresponding to surface and subsurface Vo.

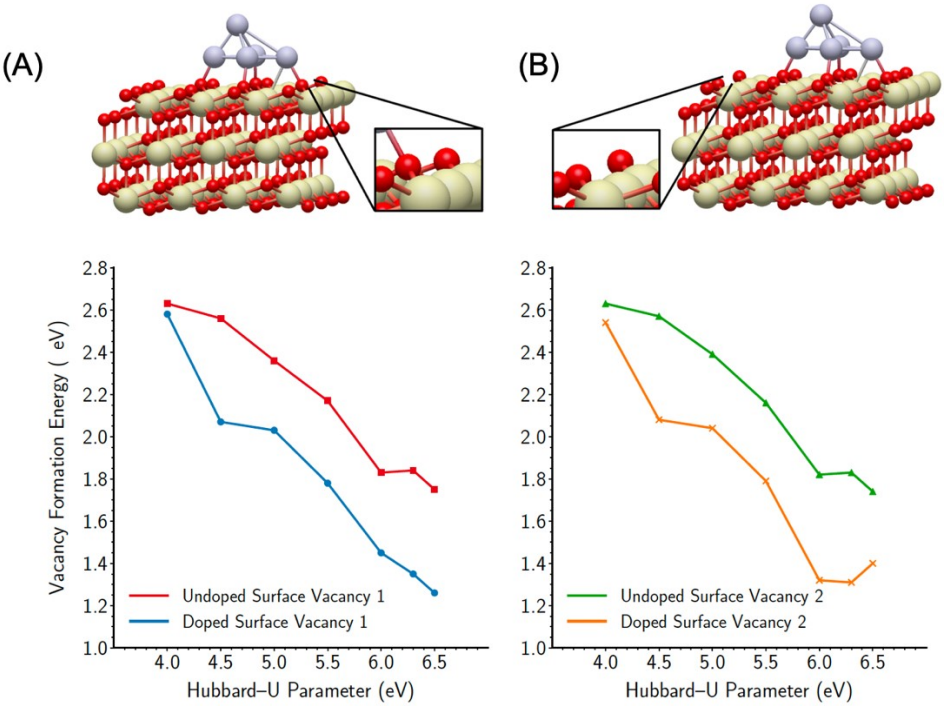

Fig. S7 Dependence of Hubbard U of the oxygen vacancy formation energy (E_{Vo}) calculation for bare CeO_2(111) surface (red line in (A) and green line in (B)) and Ag_5/CeO_2 surface (blue line (A) and orange line in (B)). Two different positions of Vo are presented in (A) and (B).

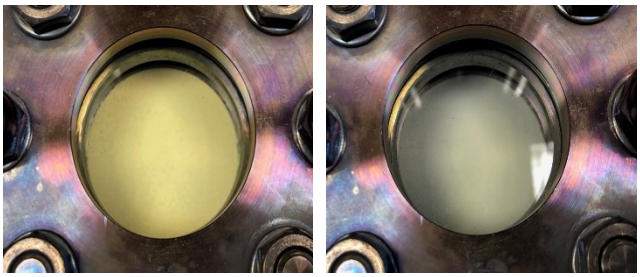

Fig. S8 Picture of CeO_2/Ag_5 AQCs on a sintered plate, (a) after oxidation on air, (b) after reduction in CH_4.

Note 1. Zoom of the XRD of the sample CeO_2/Ag_5 AQCs shown in Figure 4B – see Figure below- indicates that the sample contains metallic silver as a minor phase ≈ 0.35 (±0.1) wt%. This is due to the presence of silver ions, which are always present at the end of the clusters` synthesis (and are later reduced when deposited onto the oxide), as was reported before (see *e.g.* references 7 and 36 of the main text). Silver ions are usually precipitated with NaCl, but there is always a remaining proportion of unprecipitated Ag^+ in the final samples. In any case, we carried out blanks using $AgNO_3$ (with a total loading of 0.5 wt%) in the experiments and we did not observe any catalytic activity. Because the total Ag loading is 0.5 wt%, the "true" loading of Ag_5 clusters in the experiments should be ≈ 0.15 wt%, but we did not take such small correction into account.

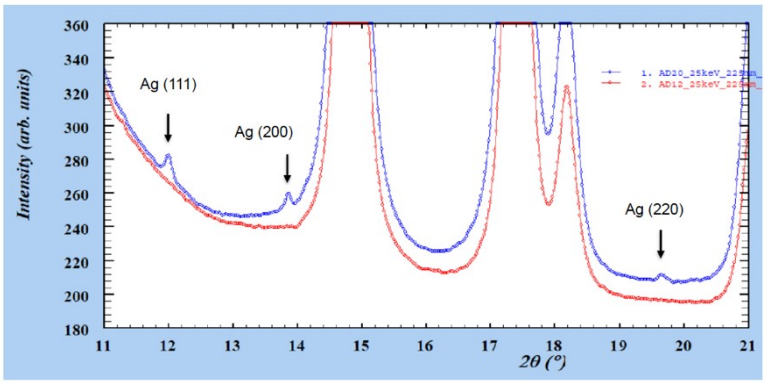

Note 2. Figure below shows the crystallite size of the fluorite structure as a function of time and gas atmosphere at an isothermal temperature of 450 ºC: reduction and oxidation periods are indicated by green and red colors, respectively. As observed, the crystallite size of the fluorite structure in the CeO_2 sample remains constant over time and under both atmospheres, suggesting inactivity of this sample. In contrast, the CeO_2/Ag_5 AQCs sample exhibits a significant increase in crystallite size over time during the reduction phase (switching to H_2 before stabilizing during the oxidation phase). The crystallite size increases from 7 nm at the start of the experiment to approximately 11 nm by the end. This increase in crystallite size suggests grain growth of CeO_2 during the reduction step.

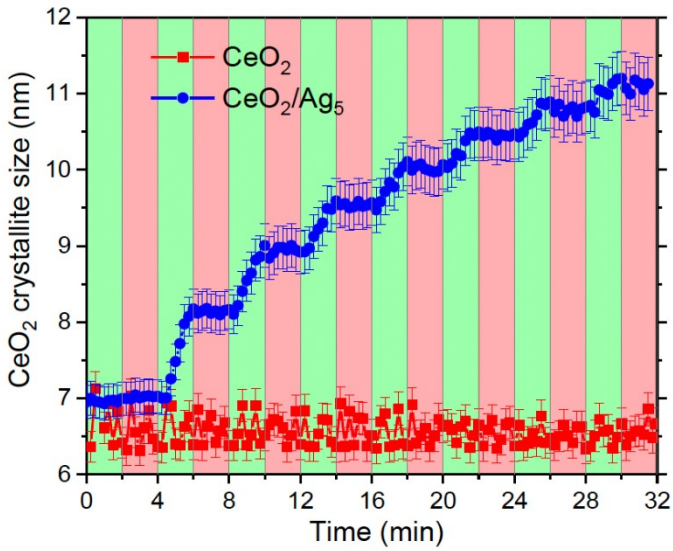

Table S1 Results of the deconvolution of the XPS spectra.

Sample	Ce^{4+}						Ce^{3+}		Concentration	
	v	v''	v'''	u	u''	u'''	v_0	u_0	$\%Ce^{3+}$	$\%Ce^{4+}$
Before irradiation	195475.0	144985.0	194099.0	127785.0	88629.9	143023.0	184657.0	129079.0	26.0	74.0
After red. With light	57625.6	25301.1	63482.9	40926.6	12779.9	40449.2	111671.0	51139.4	40.4	59.6
After red. With methane	134989.0	68066.0	144283.0	99113.0	40613.0	94976.4	275760.0	155621.0	42.6	57.4

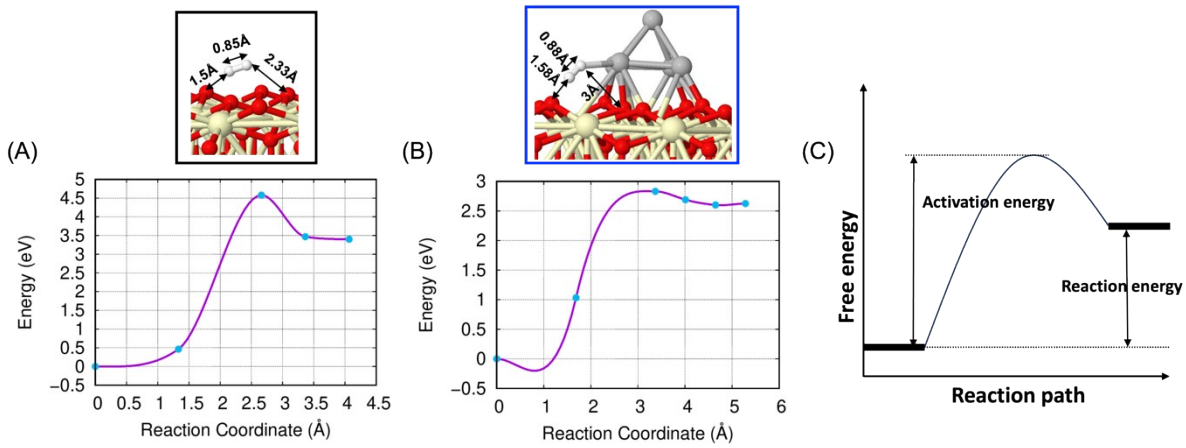

Fig. S9 Configurations of the transition states and the reaction paths for H_2 forming from separate [H]s on the reduced CeO_2 surface in the absence (A) and presence (B; site 6) of pyramidal Ag_5 AQC.

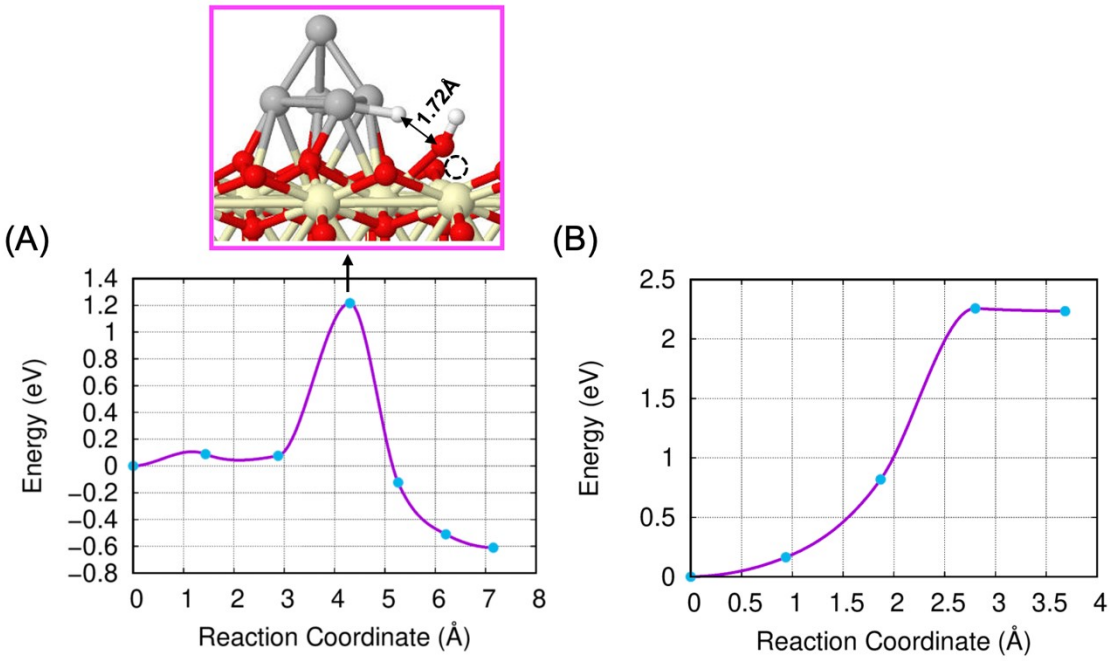

Fig. S10 Energetics of H_2O splitting (A) and H_2 forming (B) on bipyramidal Ag_5/CeO_2. The corresponding configuration of the transition state (TS) is shown in the upper panel.

Note 3. STH calculation.

STH was calculated by the following equation (adapted from M. Romero et al. *Energy Environ.Sci.* 2012, **5**, 9234-9245; doi.org/10.1039/C2EE21275G)

$$\text{Efficiency (\%)} = \frac{\left[\text{chemical energy produced}\right]}{\left[\text{energy input}\right]} = \frac{\left[\text{rate } H_2 \text{ production}\right]\left[\Delta G^{\circ}_{fH2O}\right]}{\left[\text{Solar input} + \text{Thermal input}\right]} \times 100$$

Data (per cycle of 2h) (ΔG = 285,8 kJ/mol)

Rate H_2 production: 4.91 mg

Energy produced: 4.91/(2*1000) mol *285.8 kJ/mol= ***0.7 kJ***

E solar input: 0,25 J $s^{-1}cm^{-2}$ *7200s/1000 = *1.8 kJ* (window = $1cm^2$)

E thermal input: $E_{CZO} + E_{water} + E_{H2} + E_{Ar}$ (from 25ºC to 600ºC)

E_{CZO} = 2.727g*0.48J/g-K*575K/1000 =**0.75 kJ**

Water injected (liquid): 10 µL /min x 110min = 1100 µL = 1.1 mL = 1.1g

E_{water} = [1.1 g*(4.18J/g-K*75K+2260J/g +2J/g-K*500K)/1000] = **3.93 kJ**

H_2 injected: 2 mL/min * 10 min = 20 mL

E_{H2} = (0.020L/22.4) mol*28.8 J/mol-K*575K/1000) = **0.01 kJ**

Ar injected: (28mL/min *10min (1st step) + 10 mL/min*110min)/1000 = 1.38L

E_{Ar} = (1.38 L/22.4) mol * 20.8J/mol-K * 575K)/1000 = **0.74kJ**

E thermal input = 0.75kJ+3.93kJ+0.01kJ+0.74kJ = *5.44kJ*

E_{TOTAL} input = *5.43kJ* + *1.8kJ* = ***7.24 kJ***

Then, the **STH** = (0.7/7.24) *100 **= 9.7%**

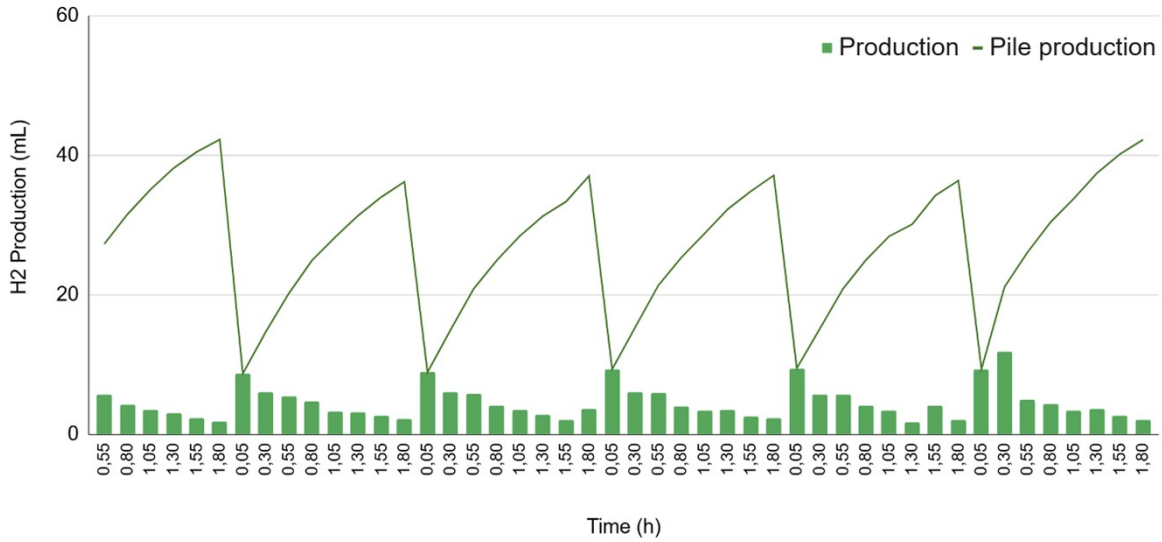

Fig. S11 Thermal contribution at 600ºC. Average net production without light at 600ºC: 17.76 mL (2h) or 8.9 mL/h

Temperature ºC	H_2 net production mL/h
600	27.5
500	4.4
450	2.0

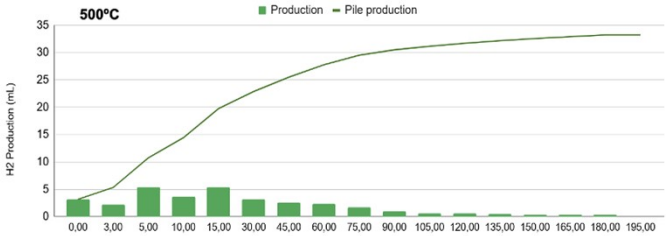

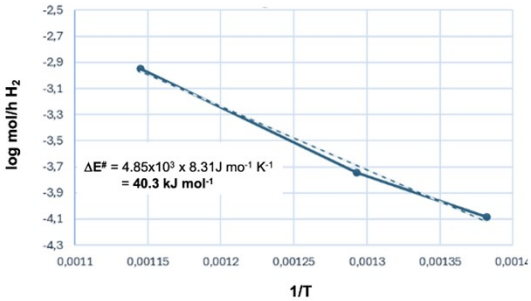

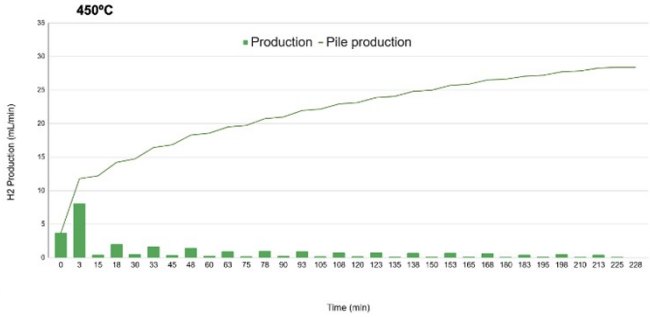

Fig. S12 Net H_2 production at different temperatures, at the same experimental conditions given in Fig.8, and the corresponding activation energy of the process.

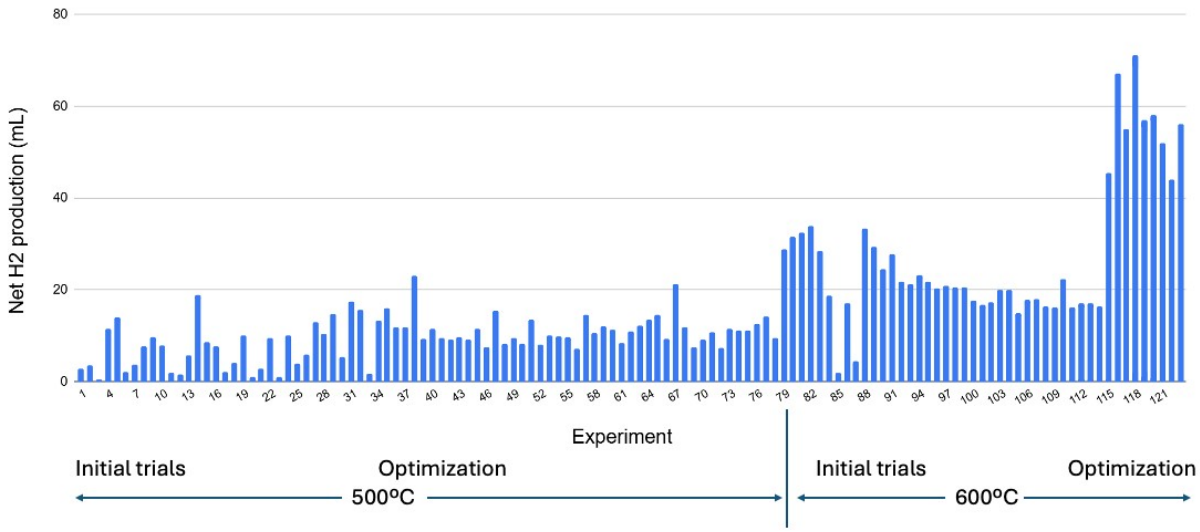

Fig. S13 Initial trials and optimization experiments at 500ºC and 600ºC using an optimized H_2-assisted method with $Ce_{0.5}Zr_{0.5}O_2/Ag_5$ AQCs (0.5%); m $Ce_{0.5}Zr_{0.5}O_2$ = 2.727g. Sample

was stable for more than ≈ 370h: 124 cycles (78 at 500ºC and 46 at 600ºC) x 3h average time per cycle. Data are available at the following link: Data optimized HEL

(Note: poor production in some cycles was due to different failures in the experiments, such as broken O-rings, failures in the water syringe supplier, air leaks inside the reactor, etc).

Studied experimental conditions:

- H_2 flow in the first step: from 1 mL/min to 10 mL/min, changing flow time from 2 min to 60 min
- Ar flow: 1st step: 20 mL/min to 29 mL/min; second step: 10 mL/min to 30 mL/min
- Water flow in the second step: from 5 mL/min to 10 mL/min.
- In some cases, an intermediate Ar flow of 20 mL/min (from 30 min to 60 min) was introduced to study the influence of the separation of the 1st and 2nd step.

Table S2 Comparison of the best representative results obtained for Ce-based oxides, perovskites, aluminates and entropy stabilized oxides, reported in the literature for the thermochemical hydrogen (STCH) production, with our photo-thermochemical looping process.

Material	T (ºC)	H_2 (μg g^{-1} h^{-1})	Reference
CeO_2	1400	60	Le Gal et al.,10.1021/ef4014373 (2013)
CeO_2	1350	118	Barcellos et al., 10.1039/c8ee01989d (2018)
$Ce_{0.46}Zr_{0.54}O_2$	1400	260	Le Gal et al.,10.1021/ef4014373 (2013)
$Ce_{0.46}Zr_{0.54}O_2$	1300	118	Le Gal et al.,10.1021/ef4014373 (2013)
$Ce_{0.75}Zr_{0.25}O_2$	1200	240	Le Gal et al.,10.1021/ef200972r (2011)
$Ce_{0.75}Zr_{0.25}O_2$	1000	197	Le Gal et al.,10.1021/ef200972r (2011)
$Ce_{0.2}Sr_{1.8}MnO_4$	1400	602	Barcellos et al.,10.1021/acs.inorgchem.8b03487 (2019)
$Sr_{0.4}La_{0.6}Mn_{0.6}Al_{0.4}O_3$	1350	541	Barcellos et al., 10.1039/c8ee01989d (2018)
$SrTi_{0.5}Mn_{0.5}O_3$	1400	494	Qian et al., 10.1021/acs.chemmater.0c03278 (2020)
$BaCe_{0.25}Mn_{0.75}O_3$	1350	353	Barcellos et al., 10.1039/c8ee01989d (2018)
$(La_{0.8}Sr_{0.2})(Mn_{0.2}Fe_{0.2}Co_{0.4}Al_{0.2})O_3$	1350	790	Zhang et al., 10.1021/acs.chemmater.2c03054 (2023)
$CaTi_{0.5}Mn_{0.5}O_3$	1350	595	Qian et al., 10.1016/j.matt.2020.11.016 (2021)
$FeAl_2O_4$	1450	720	Hoskins et al., 10.1016/j.apenergy.2019.04.169 (2019)
$La_{0.8}Al_{0.2}NiO_3$	800	429	Perez et al., 10.1016/j.cattod.2021.12.014 (2021)
(FeMgCoNi)O	1300 & 1100	1000 & 150	Zhai et al., 10.1039/c8ee00050f (2018)
$Ce_{0.5}Zr_{0.5}O_2/Ag_5$	600	435	Our photo-thermochemical process

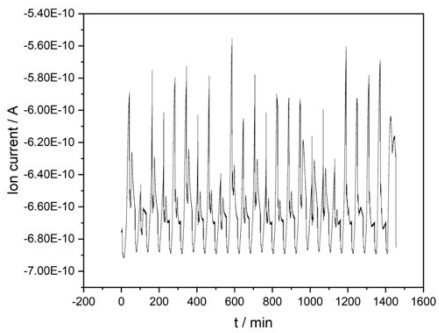

Fig. S14 m/z = 2 signal from HEL loop with CeO_2 / Ag_5 AQCs as catalyst and CH_4 as reducing agent, reaction conditions : m = 50 mg, $A_{irradiation}$ = 19.6 cm^2 , dV/dt = 15 ml min^{-1} with 2 : 1 Ar : CH_4 for the reduction cycle, dV/dt = 13 ml min^{-1} with 10 : 3 Ar : H_2O, T = 773 K, Irradiation source: 1000 W Xe lamp, $t_{Oxidation}$ = 0.5 h, $t_{Reduction}$ = 0.5 h

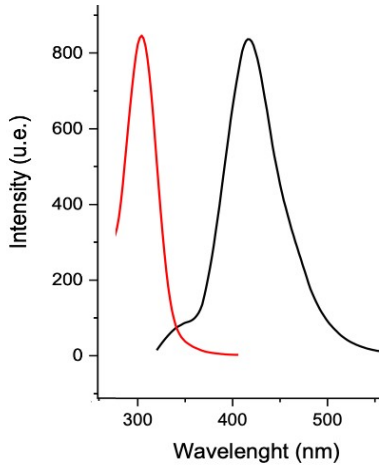

Fig. S15 Excitation (red, 300 nm) and emission (black, 409 nm) peaks of the electrochemical synthesized Ag_5 AQCs.

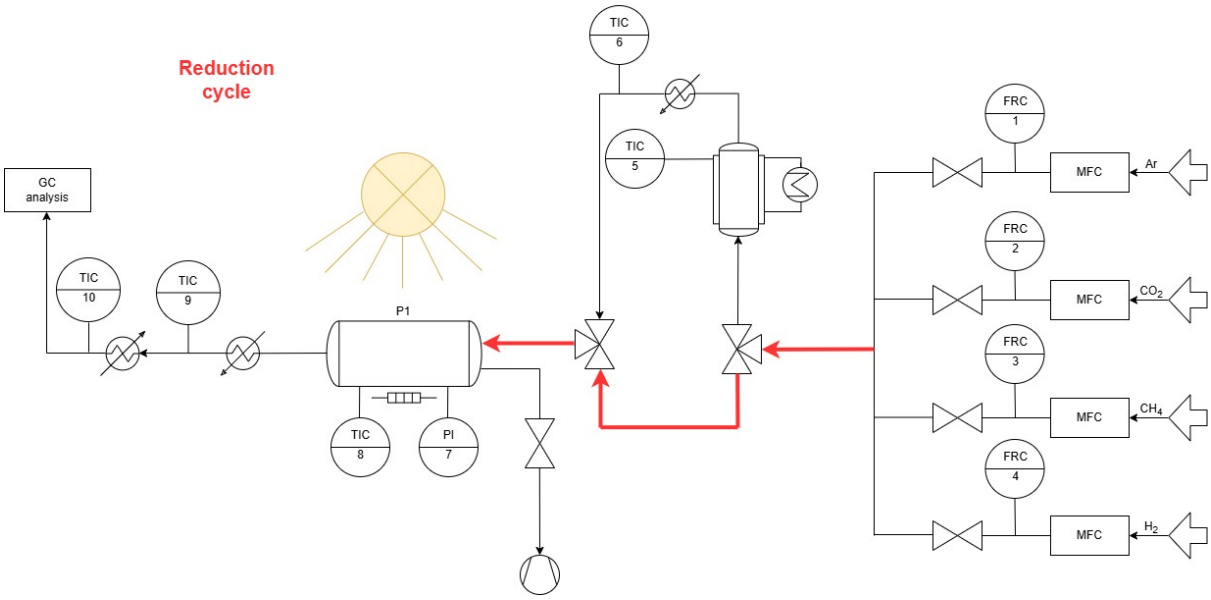

Fig. S16a Flow chart of the setup in the reduction cycle (light is introduced through a quartz window from the top).

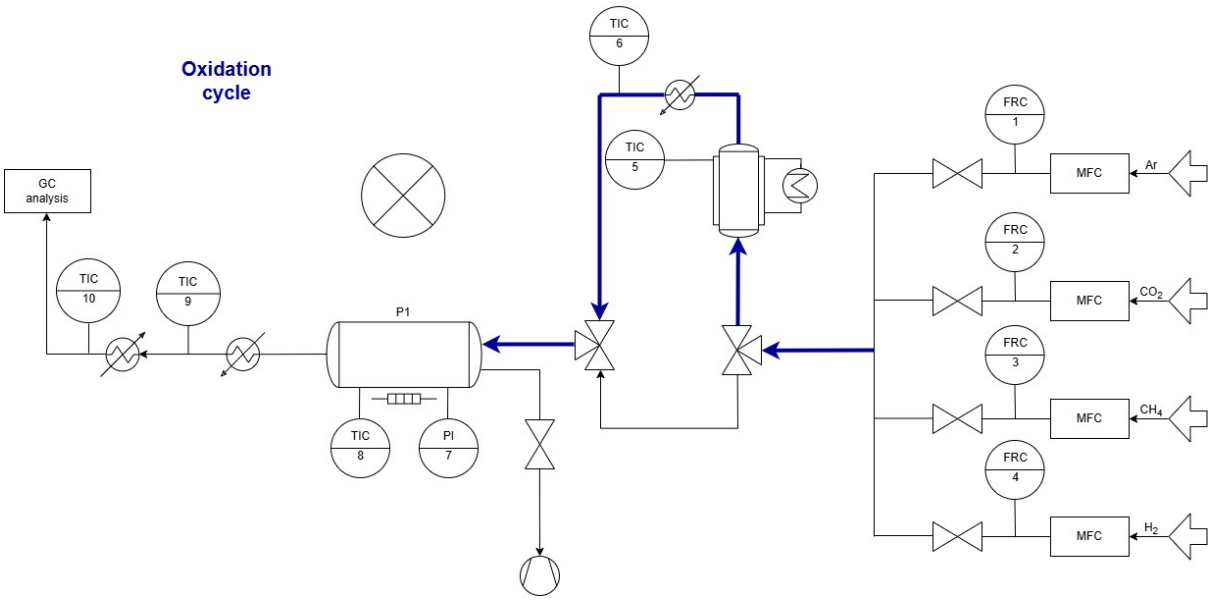

Fig. S16b Flow chart of the setup in the oxidation cycle (without light).